# Characterization of Dense Arrays of Chemiresistor Vapor Sensors with Submicrometer Features and Patterned Nanoparticle Interface Layers

Forest I. Bohrer,[†,‡] Elizabeth Covington,[§] Çagliyan Kurdak,[§] and Edward T. Zellers[*,†,‡]

Center for Wireless Integrated Microsystems, [†]Department of Environmental Health Sciences, [‡]Department of Chemistry, and [§]Department of Physics, University of Michigan, Ann Arbor, Michigan 48109-2029, United States

S *Supporting Information*

ABSTRACT: The performance of arrays of small, densely integrated chemiresistor (CR) vapor sensors with electron-beam patterned interface layers of thiolate-monolayer-protected gold nanoparticles (MPNs) is explored. Each CR in the array consists of a $100\text{-}\mu m^2$ interdigital electrode separated from adjacent devices by 4 μm. Initial studies involved four separate arrays, each containing four CRs coated with one of four different MPNs, which were calibrated with five vapors before and after MPN-film patterning. MPNs derived from *n*-octanethiol (C8), 4-(phenylethynyl)-benzenethiol (DPA), 6-phenoxyhexane-1-thiol (OPH), and methyl-6-mercaptohexanoate (HME) were tested. Parallel calibrations of MPN-coated thickness-shear-mode resonators (TSMR) were used to derive partition coefficients of unpatterned films and to assess transducer-dependent factors affecting responses. A $600\text{-}\mu m^2$ 4-CR array with four different patterned MPN interface layers, in which the MPN derived from 7-hydroxy-7,7-bis(trifluoro-methyl)heptane-1-thiol (HFA) was substituted for HME, was then characterized. This is the smallest multi-MPN array yet reported. Reductions in the diversity of the collective response patterns are observed with the patterned films, but projected vapor discrimination rates remain high. The use of such arrays as ultralow-dead-volume detectors in microscale gas chromatographic analyzers is discussed.
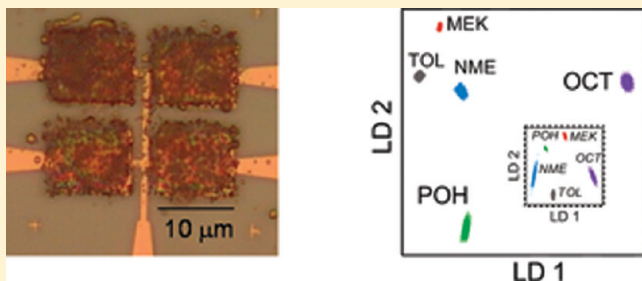
T hiolate-monolayer-protected gold nanoparticles (MPNs) have been used as vapor-sorptive interface layers on a variety of transducers, including thickness shear mode resonators,[1] surface acoustic wave devices,[2] optical sensors,[3] and, most commonly, chemiresistors (CRs).[4–10] Electronic conduction in MPN films occurs by field-induced tunneling, and has been modeled successfully using insulated granular metal (cermet) theory, in which the resistivity is expressed as a function of the Au-core radius (r), the intercore distance (δ), the electronic tunneling coefficient (β), and the dielectric constant of the intercore matrix (ε_{th}).[11] Reversible sorption of vapors causes δ to increase and may also change ε_{th}, which usually produces transient increases in MPN film resistance. It has been demonstrated with alkane-thiolate MPNs that CR responses to a given mass of sorbed vapor vary with the density and dielectric constant of the analyte, and the swelling efficiency of the MPN film.[9]

By incorporating a set of MPNs having different thiolate structures in a CR array, each sensor responds to a different extent to a given vapor and the collective response pattern produced permits the discrimination of individual vapors and the components of simple mixtures.[8,12,13] Use of such an array as the detector in a mesoscale or microscale gas chromatograph (μGC) permits the analysis of complex vapor mixtures at low concentrations;[14] the combination of retention times and array response patterns enhances the reliability of analyte determinations.

Since the responses of MPN-coated CRs depend on partitioning of vapors into the MPN film, they vary in proportion to the concentration of vapor in the headspace of the sensor. As a result, the amount of sorbed analyte required to produce a given response is proportional to the volume of the film. Therefore, miniaturization is possible without loss of sensitivity;[4b,9] using smaller CRs should permit detection of smaller quantities of analytes.[10,15,16]

In order to capitalize on the favorable scaling properties of such sensor arrays, a method for creating films of different MPNs on each of several tightly spaced sensors in a miniature array is needed. This, in turn, requires a means of patterning MPN films on each sensor with high spatial resolution. Methods reported for patterning MPNs include use of lithographically defined sacrificial layers,[17] microcontact printing,[6b] dip-pen nanolithography,[18] and electron-beam induced cross-linking (EBIX).[8,19] The first of these is not amenable to patterning multiple MPN layers, and the dip-pen technology would require a prohibitively long period of time to cover the areas of interest ($\sim$100 μm^2) with just an initial monolayer. Of the two remaining methods, we elected to study EBIX because it offers potentially greater precision and flexibility, in addition to the possibility of imparting additional robustness to the sensor films by virtue of the cross-linking process.

EBIX can render films of alkanethiolate MPNs insoluble while retaining the Au core size and only slightly reducing the intercore

spacing (δ).[19] In a recent study, we demonstrated the feasibility of creating MPN-coated CR arrays with EBIX-patterned films of MPNs having several different functionalized thiolate monolayers.[8] In that study, however, the MPN films were tested on an array of relatively large interdigital electrodes (IDE, finger spacing = 15 μm; device area = 1.66 mm^2) that were widely separated (device spacing = 1 mm; array area = 12.8 mm^2), and on which the films of different MPNs were patterned simultaneously. In a more recent short communication, we demonstrated the process of sequentially depositing, irradiating, and developing different MPNs on an array of closely spaced IDEs with submicrometer electrode features (i.e., IDE fingers and spaces ~125 nm; device area = 100 μm^2), and showed that the array provided different responses to a pair of test vapors.[5]

In the present study we provide a more thorough characterization of EBIX-patterned MPN films on these densely integrated arrays of CRs. Five different MPNs are studied, including two for which the pre- and post-EBIX sensing behavior has not yet been explored. Mass uptake by unpatterned MPN films, as measured with thickness shear mode resonators (TSMR), is used to derive partition coefficients and to explore differences in vapor- and transducer-specific relative responses. Measurements collected from CR arrays in which all of the sensors are coated with a single type of MPN are analyzed first to assess the efficiency and reproducibility of the EBIX process, and to compare vapor response characteristics before and after patterning. Differences in vapor sensitivity upon patterning are rationalized qualitatively in terms of likely changes in thiolate structures and consequent vapor—film interactions. The impact of patterning on vapor recognition and discrimination is evaluated using chemometric analyses. Then, an integrated array with four different patterned MPNs, occupying an area of only 600 μm^2, is characterized.

■ EXPERIMENTAL SECTION

Device Fabrication. The CR arrays used in this study consist of four IDEs arranged in a 2 × 2 pattern. Each IDE contains 20 pairs of fingers 10 μm long with 150-nm widths and spaces, corresponding to a device area of ~100 μm^2. Adjacent IDEs are separated by 4 μm. The IDE patterns were defined by electron-beam lithography, and the IDEs were created by evaporating a 20-Å Ti adhesion layer followed by a 200-Å Au layer onto a thermally grown SiO$_2$ layer (~1-μm thick) on a Si substrate using a lift-off process. Diced arrays were mounted on 16-pin dual-in-line packages with indium-soldered wire contacts. The TSMRs comprise circular quartz crystals (1.4 cm in diameter) with rough gold electrodes (0.8 cm in diameter) and a resonant frequency of 10 MHz (International Crystal; Oklahoma City, OK). Right-angle header pins were soldered to TSMR device leads for electrical contacts.

Materials. MPNs were prepared using the single-phase method reported by Rowe et al.[20] Thiolate monolayers were derived from *n*-octanethiol (C8), 4-(phenylethynyl)-benzenethiol (DPA), 6-phenoxyhexane-1-thiol (OPH), methyl-6-mercaptohexanoate (HME), and 7-hydroxy-7,7-bis(trifluoro-methyl)heptane-1-thiol (HFA).[8] Nanoparticle diameters were determined from TEM images, and range from 3.4 nm (DPA) to 4.7 nm (HME) with relative standard deviations (RSD) of 5—23%. Purified MPNs were dissolved in appropriate solvents (toluene for C8, OPH, and DPA, 2-butanone for HME and HFA) at concentrations of 5—6 mg/mL for storage and deposition. Analytes included the following volatile
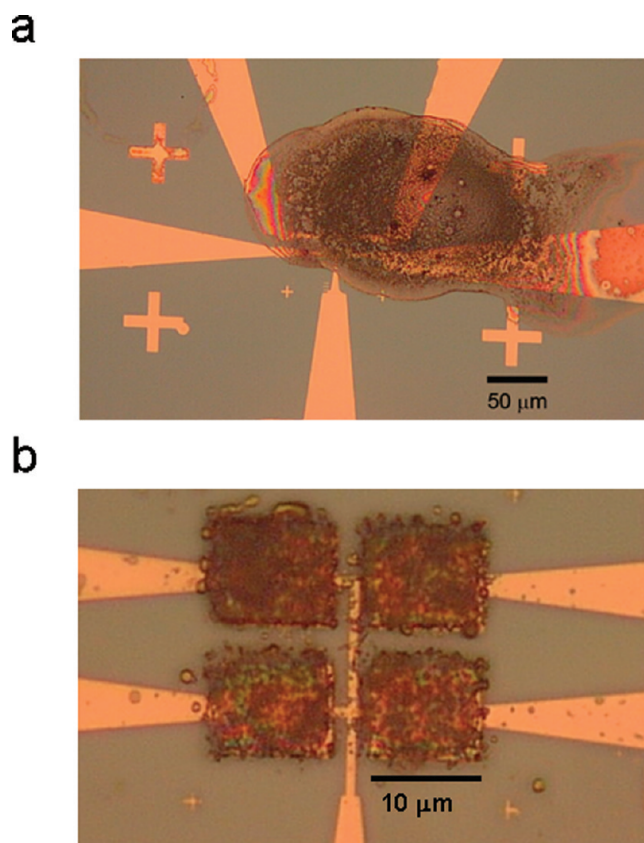

Figure 1. (a) Optical micrograph of microdispenser-printed OPH-MPN film covering all four CRs in a mono-MPN array. (b) Optical micrograph of the same mono-MPN array with patterned OPH$_x$ films.

organic compounds (VOCs): toluene (TOL), *n*-propanol (POH), 2-butanone (MEK), *n*-octane (OCT), and nitromethane (NME). All compounds were purchased at analytical purity (99.5+%, Fisher Scientific) and dried over 4 Å molecular sieves before use.

Film Deposition. Prior to MPN film deposition all devices were cleaned by sequential sonication in acetone and 2-propanol followed by drying in a scrubbed-air stream. Arrays were coated from solution by use of a precision droplet microdispensing system (Jetlab 4, MicroFab, Plano, TX). Upon drying, the resulting MPN films were generally circular with a radius of ~150 μm, such that a single droplet could cover all four IDEs (Figure 1a).[5] A test film of OPH gave an average thickness of 240 nm (standard deviation = 130 nm) by AFM across all four sensors (Figure 1b), and since similar MPN solution concentrations, microdispenser settings, and procedures were used for all MPNs, it is assumed that all film thicknesses were similar to this value.[5]

TSMR devices were coated by airbrushing the MPN solutions with pressurized air as propellant. Recorded frequency shifts ranged from 11.8 to 13.5 kHz, corresponding to film masses of 24 to 28 μg (via Sauerbrey equation). Assuming a nominal density of 4.3 g/cm^3,[13] these masses correspond to average thicknesses of 116 to 136 nm, which are within the acoustically thin regime.[1]

Film Patterning. MPN films were cross-linked with a scanning electron microscope (Philips XL30 FEI, Hillsboro, OR) at a dose of 600 μC/cm^2 and potential of 30 keV, with a beam diameter of ~20 nm and spot-to-spot distance of <20 nm. The films were then developed by sequentially rinsing with toluene,

acetone, and 2-propanol to remove any un-cross-linked material.[5] Patterned films will henceforth be denoted with a subscript x to differentiate them from unpatterned films of the same MPN (e.g., $C8_x$ vs C8). Four separate arrays were prepared, each coated with a single type of MPN (e.g., C8) on all four IDEs in order to study the changes in sensor characteristics incurred upon patterning. We refer to these as "mono-MPN" arrays in all discussions below. The films on all four of the sensors in each mono-MPN array were irradiated prior to rinsing with solvents. Since films of HFA MPNs exhibited resistances that varied widely and were typically too high to measure,[8] this material was omitted from the set of mono-MPN arrays examined.

A single CR array having a different EBIX-patterned MPN on each IDE (henceforth referred to as a "multi-MPN" array) was prepared with films of $C8_x$, DPA_x, OPH_x, and HFA_x. In this case, a film of C8 was first deposited with the Jetlab over the entire array. The area corresponding to one of the IDEs was then e-beam irradiated, and the entire array was developed by the series of solvent rinses described above to remove the C8 film from nonirradiated areas.[5] This procedure was repeated three times with a different MPN solution until each IDE in the array was coated with a different patterned MPN film. Films were deposited/patterned in the following order: $C8_x$, OPH_x, DPA_x, HFA_x. In an attempt to ensure sufficient film thicknesses, a greater amount of C8 was deposited by the microdispenser than in the mono-MPN array cases.

Vapor Exposures. Sensors were mounted in a 0.5-L stainless-steel chamber equipped with electrical feed throughs and fluidic ports, which was maintained at 25.0 ± 0.1 °C. Test atmospheres of each VOC were generated by passing scrubbed air through a fritted bubbler containing the liquid analyte, followed by dilution in a dry, scrubbed air stream. Air flow was regulated by mass flow controllers with a total chamber flow of 14 L/min. Vapor concentrations were confirmed by flame ionization detector. Calibration curves spanned a ~10-fold concentration range, with typical minimum concentrations of 2−3% of the concentration corresponding to the saturation vapor pressure, p_{sat}.

Each CR in a mono-MPN array was connected in series with a reference resistor ($R_{ref} = 3.0$ MΩ) and biased with a dc voltage from a battery ($V_A = 1.59$ V). The voltage drop across the CR (V_S) was measured by a digital voltmeter with multiplexer card (model 34970A/34902A, Agilent Technologies, Santa Clara, CA) and recorded with Agilent software on a PC. The sensor resistance (R_S) was calculated via the equation $R_S = (V_S R_{ref})/(V_A - V_S)$.[9] The output from each CR in the multi-MPN array was measured by recording the ac current using a lock-in amplifier (SR830, Stanford Research Systems, Sunnyvale, CA) and then converting to resistance; each sensor was calibrated individually.

TSMR sensors were mounted between Viton o-rings in a custom stainless steel holder fabricated in-house so that the sensing area of the TSMR was exposed to the test atmosphere while the rest of the crystal was isolated.[9] The holder was then mounted in the lid of the exposure chamber. Sensor frequencies were monitored by a phase-lock oscillator (Maxtek, Beaverton, OR) and recorded with Maxtek software on a PC.

Statistical Methods. Linear discriminant analyses were performed using the R statistical computing environment (version 2.9.2, Auckland, New Zealand). Monte Carlo simulations were performed in both Microsoft Excel 2007 and Visual Basic 7.0. Extended disjoint principal component regression (EDPCR) classification routines developed in-house were run in Visual Basic 7.0. The technical details of our use of Monte Carlo simulations with EDPCR analyses of sensor array response patterns have been described elsewhere.[12]

RESULTS AND DISCUSSION

Unpatterned MPN Film Resistances. The CR baseline resistance values, R_b's, of unpatterned MPN films can be used together with published data on monolayer structures and ligand overlaps to characterize certain features of the films. The average R_b values and standard deviations ($n = 4$) for the C8, DPA, OPH, and HME mono-MPN arrays were 1.16 ± 0.02, 1.10 ± 0.36, 15.9 ± 4.3, and 12.3 ± 5.6 MΩ, respectively. The R_b values for the C8 devices are remarkably similar (i.e., relative standard deviation, RSD, < 2%), while those for the DPA, OPH, and HME devices are more variable (i.e., RSDs of 30−40%), presumably due to small variations in MPN ordering in the multilayer films.

The ligands on adjacent C8 MPNs are known to intercalate significantly. Assuming full, surface-normal extension of the octanethiolates, δ_{C8} is ~1.2 times the ligand length (14.7 Å), or 17.6 Å.[9,21] The OPH ligands form approximately surface-normal, densely packed, ordered 2-dimensional films on planar Au, with significant $\pi-\pi$ interactions between adjacent phenyl groups.[22] By analogy with phenylalkyl thiolate ligands on MPNs,[11] δ_{OPH} should be ~1.7 times the reported ligand length (15 Å),[22] or 25.0 Å. The average OPH R_b value, while much higher than that for C8, is lower than expected theoretically for a fully insulating intercore matrix with this value of δ_{OPH}. This suggests that the phenyl groups are acting as tunneling bridges between adjacent gold cores and reducing the energy of the tunneling barrier.[11]

The length of the DPA ligand is 15.6 Å,[23] and δ_{DPA} was estimated from images in ref 20 to be 20 Å (i.e., 1.3 times the ligand length).[20] While the nominal δ_{DPA}:δ_{C8} ratio is 1.15, the R_b values for C8 and DPA films are nearly equivalent, owing to the high degree of conjugation in DPA which facilitates electron tunneling.[11,20,23] Although MPNs with ester ligands, such as HME, have not been studied in detail, spectroscopic analysis of the interaction of methyl acetate with polyester films in the solid state indicates antiparallel dipole−dipole association of the carbonyl groups.[24] Assuming that similar interactions dictate the intercalation of HME MPNs, δ_{HME} should be ~1.5 times the ligand length (12.7 Å), or 19.3 Å. This corresponds to a δ_{HME}:δ_{C8} ratio of 1.11, and an expected 9-fold difference in R_b, which is close to the 11-fold average difference observed.

Response Isotherms with Unpatterned MPN Films. CR and TSMR sensors coated with unpatterned MPNs exhibited rapid, reversible responses to vapor challenges, with full response and recovery achieved in less than 30 s. The observed time constants of 4−9 s are on the order of the chamber mixing time (6.5 s) and are consistent with those observed previously.[8,9] Response times did not differ significantly among the CR sensors and vapors tested. By convention, we report CR responses as the change in resistance upon vapor exposure, ΔR (from ΔV), normalized by R_b, and then multiplied by 10^6 (R_{ppm}). TSMR responses are reported in a similar manner as the change in frequency, Δf, normalized by the frequency change due to film deposition, f_f, and multiplied by 10^6 (f_{ppm}). Calibration curves generated for the CRs and TSMRs with unpatterned MPN films are linear, with forced zero regression values $r^2 \geq 0.98$, in all cases.

3689

dx.doi.org/10.1021/ac200019a |Anal. Chem. 2011, 83, 3687–3695

Table 1. Vapor Pressures, Partition Coefficients, and Sensitivity Ratios of All Sensors

	MEK	NME	TOL	POH	OCT
Vapor Pressure[a] (torr)					
	95.3	35.8	28.4	21.0	14.1
Partition Coefficients (K)[b]					
C8	75	140	720	420	1300
DPA	180	450	1600	810	1800
OPH	110	360	710	320	550
HME	75	230	650	340	950
CR/TSMR Sensitivity Ratios (Unpatterned MPN Films)[c]					
C8	41	50	46	40	95
DPA	2.9	1.7	2.6	3.5	1.6
OPH	77	49	91	85	51
HME	33	32	55	45	18
CR_x:CR Sensitivity Ratios (Patterned/Unpatterned)[d]					
C8	0.70	0.40	0.37	0.86	0.16
DPA	2.7	3.6	1.4	3.2	2.2
OPH	0.41	0.57	0.23	1.0	0.33
HME	1.5	1.1	0.39	1.9	0.66

[a] From ref 36 (25 °C). [b] Determined using MPN densities of 4.3, 4.2, 5.2, and 4.3 g/mL for C8, DPA, OPH, and HME, respectively, derived from data in refs 9 and 20. [c] Ratios used vapor concentrations in mg m^{-3} and the average CR sensitivities. [d] Ratio of average sensitivities of the mono-MPN arrays (patterned/unpatterned).

Partition coefficients, K, were determined from TSMR calibrations via eq 1 and are listed in Table 1[1,25]

$$K = \frac{\rho_f \Delta f}{f_f C} \qquad (1)$$

where C is the air concentration of the analyte vapor in mass per unit volume, and ρ_f is the density of the MPN film. Values of K for TOL, POH, and OCT in C8 reported previously[9] are similar (i.e., within 28%) to those in Table 1. Notably, the K values for the test vapors with DPA are consistently higher than those for C8, OPH, and HME. This can be explained, in part, by the larger mass percentage of organic material in the DPA MPN (24%) compared to those in C8, OPH, and HME (i.e., 16%, 17%, and 20%, respectively).[20]

TSMR sensitivities are presented in terms of the mass-per-unit-volume vapor concentration (f_{ppm}/mg m^{-3}) in Figure 2a and in terms of the percentage of the saturation vapor pressure (i.e., f_{ppm}/%p_{sat}) in Figure 2b. The former are directly proportional to the K values (eq 1) and are dictated primarily by the analyte vapor pressure, with the intermolecular interactions between the vapors and thiolate monolayers exerting secondary effects. Accordingly, the sensitivities generally increase from left to right for all of the sensor films in Figure 2a, in order of decreasing analyte vapor pressure. The exception is POH, for which sensitivities are lower than expected due to its significant dipolarity and hydrogen-bonding strength, which reduce its vapor pressure as well as its vapor-phase affinity for the less polar MPN films.

Using the latter expression for sensitivity removes the influence of vapor pressure, such that the intermolecular interactions should be more apparent in the sensitivity patterns (Figure 2b).

The higher sensitivities exhibited toward TOL and OCT for all of the sensors in Figure 2b reflect the typical predominance of dispersive forces in all nonbonding vapor–film interactions. This is most apparent for the nonpolar C8 MPN. The higher sensitivities for TOL with the DPA and OPH sensors reflect the additional influence of polarizability and π–π interactions.[26] Given the hydrogen-bond basicity and dipolarity of the ester tail group,[27] it is surprising that the TOL sensitivity with the HME sensor is so much higher than the sensitivities for the more polar POH, MEK, and NME vapors. However, binary mixtures of methyl esters with aromatic compounds, in fact, show very low excess molar enthalpies (heats of mixing),[28] most likely from n–π interactions between the unpaired electrons of the carbonyl oxygens and the aromatic ring, which may explain the higher HME sensitivity to TOL. This result, coupled with the higher relative sensitivity of HME to OCT as compared to the polar analytes (Figure 2b), suggests further that the carbonyl groups on adjacent ligands are self-associating and reducing the effective dipolarity and hydrogen-bonding strength expected from the free ester group. This is accordant with the arguments presented above relating R_b and δ_{HME} to the ligand overlap in the HME films.

Transducer-Related Sensitivity Differences. CR sensitivities were taken as the average slopes of the calibration curves from the four sensors in the mono-MPN arrays and are presented in units of R_{ppm}/mg m^{-3} in Figure 2c. Among the CRs in a given mono-MPN array, vapor-specific sensitivities are quite reproducible, with RSDs < 9.5% in all cases. For a given sensor, the average RSD of the sensitivities derived from the slopes of the calibration curves for all vapors ranged from 3.2% to 5.1%. Limits of detection are provided and discussed in the Supporting Information.

The similarities in the relative CR and TSMR sensitivities among the vapors with a given MPN are apparent by visual comparison of the sensor-wise patterns shown in Figure 2a,c. However, the correlation (r^2) varies from 0.65 for HME to 0.94 for C8. The TSMR depends only on the added vapor mass, while the CR depends on the volume occupied by the (condensed) vapor, its dielectric constant, and the efficiency with which the MPN is swelled by the sorbed vapor (i.e., the change in film volume per unit volume of sorbed vapor).[9] Thus, the subtle differences in the sensor-wise patterns in Figure 2a,c are not unexpected.

Furthermore, CR sensitivities are consistently higher than TSMR sensitivities (Table 1).[9] For C8, OPH, and HME, the average CR/TSMR sensitivity ratios (R_{ppm}/f_{ppm}) are in the range 18–95 and vary by as much as 3-fold among the five vapors for a given MPN. No clear correlations between these ratios and the vapor densities and dielectric constants were observed, arguing further for the importance of swelling efficiency as a cofactor influencing CR responses.[9]

The most notable feature of the CR/TSMR sensitivity ratios, however, is the very low values observed for DPA, which range from only 1.6–3.5 among the five vapors. It was noted above that the K values are consistently higher for DPA than for the other MPNs. As shown in Figure 2c, the DPA CR sensitivities, in contrast, are consistently lower than those of the other MPNs for all vapors. The rigidity of monolayers like DPA can reduce the degree of interlinkage (i.e., number of ligands interacting between adjacent Au cores) and the swelling efficiency, leading to smaller changes in intercore distance for a given mass uptake.[1] The facilitated electron tunneling provided by the highly conjugated
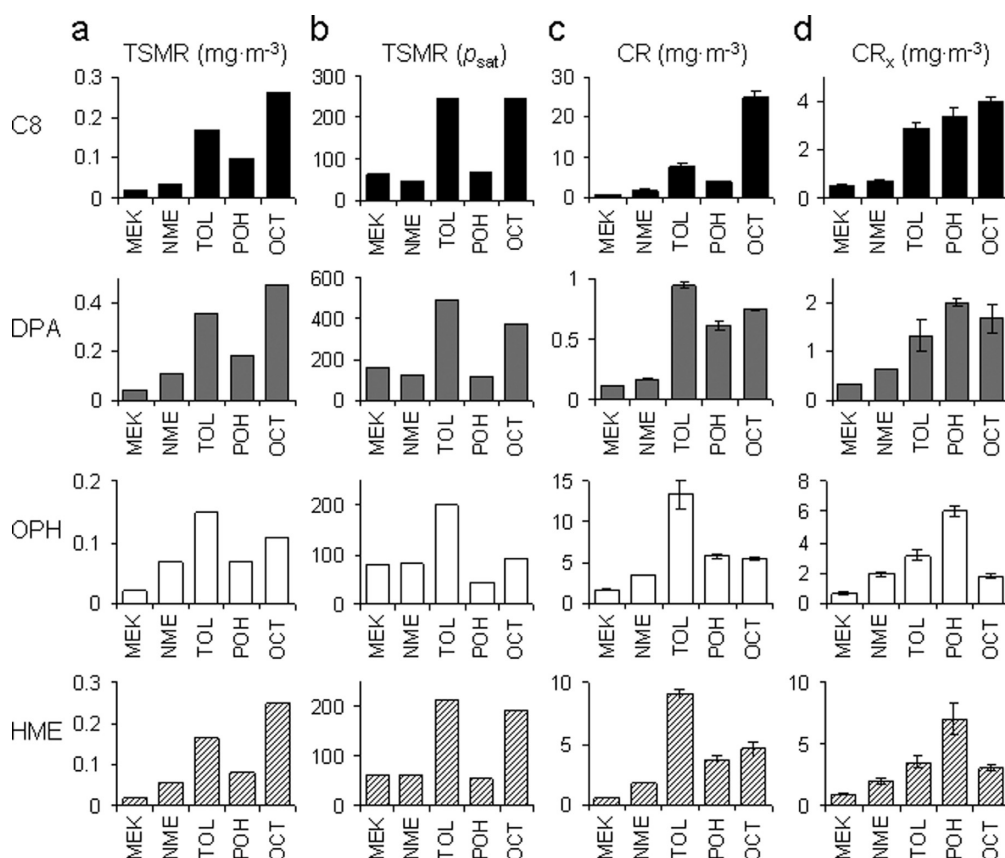
Figure 2. (a) Unpatterned MPN-film TSMR sensitivities in units of $f_{ppm}/(\text{mg m}^{-3})$. (b) Unpatterned MPN-film TSMR sensitivities in units of $f_{ppm}/\%$ p_{sat}. (c) Unpatterned MPN-film CR sensitivities in units of $R_{ppm}/(\text{mg m}^{-3})$. (d) Patterned MPN-film CR sensitivities in units of $R_{ppm}/(\text{mg m}^{-3})$. Analytes include 2-butanone (MEK), nitromethane (NME), toluene (TOL), n-propanol (POH), and n-octane (OCT), and MPNs are designated by the different bar chart fill colors/patterns: C8 and C8$_x$ in black (top row); DPA and DPA$_x$ in gray (2nd row); OPH and OPH$_x$ in white (3rd row), and HME and HME$_x$ in crosshatch (4th row).

ligands could also reduce the impact of film swelling on film resistance.[9] These results are consistent with those reported by Lu et al.[29] and by Joseph et al.[7] who performed similar experiments with MPNs having structurally analogous thiolates.

Patterned MPN Film Resistances. The films on the mono-MPN arrays were exposed to an electron-beam dose of 600 μC/cm^2 at 30 keV with the expectation that this would be sufficient to cross-link a significant fraction of the MPNs and produce dense insoluble films.[8] While the HME$_x$ films obtained were similar in appearance to the unpatterned HME films, the C8$_x$, DPA$_x$, and OPH$_x$ films were thinner than their unpatterned precursors, suggesting decreased EBIX efficiency or poor adhesion of the cross-linked films to the substrates. After patterning, R_b values for the C8$_x$, DPA$_x$, OPH$_x$, and HME$_x$ were 0.54 ± 0.24, 1.07 ± 0.22, 9.85 ± 0.36, and 2.10 ± 0.27 MΩ, respectively. (Note that, due to an electronic problem, one of the channels was lost, such that only three of the four sensors with patterned films were measurable.) The corresponding unpatterned/patterned R_b ratios are 2.2, 1.02, 1.6, and 5.9, respectively.

Although all films become less resistive after patterning, the magnitudes of reductions are smaller than the ~6-fold reductions we observed in our previous study for the two MPNs common to both studies (i.e., C8 and OPH).[8] It was argued in that report that these reductions were due primarily to decreases in δ, with changes in β and ε_{th} being possible secondary factors. Without spectroscopic analysis, the nature of the structural

changes in the MPN films cannot be determined definitively. However, some insights can be gained from the data at hand and the literature on self-assembled monolayers (SAMs) of some of the thiolates used here and their structural analogues.

For C8, the most likely mechanism of EBIX involves scission of C—H and C—C bonds, with corresponding losses of a proton and or an alkyl fragment.[30−32] Loss of a methyl end group from C8 would result in a ~9% reduction in ligand length. If this were to result in an equivalent fractional reduction in δ_{C8} it would cause an expected 5.5-fold decrease in R_b, as observed in our prior study. Alternatively, loss of a methyl or methylene proton could lead to a new C—C (or C=C) bond between an intercalated ligand from an adjacent MPN with little or no change in ligand length or δ_{C8}. Both cross-linking mechanisms are plausible. Differences in secondary electron generation rates and energies from the substrate materials (i.e., IDE dimensions and fractional metal coverage) may be important factors affecting the cross-linked products for different devices.[30] In light of the apparent reduction in film density or thickness in the C8$_x$ samples, we cannot rule out a countervailing increase in resistance from the reduction in the number of electron tunneling paths in the C8$_x$ films.

The R_b values for the DPA$_x$ films are nearly equivalent to those of the DPA films. In this case, resistance changes due to fractional changes in δ_{DPA} may be masked by the efficiency of electron transfer across the conjugated ligands on adjacent MPNs. In

addition, proton abstraction and formation of lateral C—C linkages between phenyl groups is a favorable cross-linking mechanism,[31] which would not reduce δ_{DPA} significantly. Detailed studies of low-dose EBIX of biphenyl-4-thiol SAMs confirm the importance of secondary electrons and show that dimeric species are formed through single- and double-links (C—C bonds) between adjacent phenyl rings.[32] OPH_x may also cross-link across adjacent phenyl groups, but loss of phenoxy or phenyl moieties via scission of C—O bonds is likely, and the ensuing reduction in δ_{OPH} could contribute to the 1.6-fold reduction in R_b. Here again, the reduction in tunneling pathways associated with the apparent loss of film material may offset the decrease in resistance from these factors.

HME_x exhibits the greatest decrease in R_b. Losses of CH_3 and CO_2 are established mechanisms of e-beam degradation of self-assembled monolayers of carboxylic acids.[33] Such changes would permit reductions in δ_{HME} on the order of 10%, which would account for the ~6-fold reduction in R_b observed for HME_x. As noted below, there is some evidence for an increase in the polarity of all of the patterned films, which would tend to increase ε_{th}. However, as discussed previously,[8] it would require a large change in ε_{th} to account for significant changes in R_b, so we do not believe this factor has a significant effect on the observed changes in R_b.

Effects of Patterning on CR Responses. CR sensors with patterned films give reversible responses with response times very similar to those observed with unpatterned films. Calibration curves are linear, with regression r^2 values >0.96 in all but one case, and typically >0.98 (one of the HME_x films had a reduction in sensitivity at higher concentrations, leading to an r^2 of 0.92). Sensitivities ($R_{ppm}/mg\ m^{-3}$) are presented in Figure 2d, and the patterned/unpatterned sensitivity ratios are listed in Table 1. Increased variability in sensitivity across different sensors is observed (av inter-sensor RSD = 10%). For a given sensor, the average RSD of the sensitivities derived from the slopes of the calibration curves for all vapors ranged from 3.8% to 7.8%.

Significant changes in the absolute and relative sensitivities of the mono-MPN sensors are observed as a result of patterning the MPN films. As shown in Table 1, the arrays with $C8_x$ and OPH_x films are nearly all less sensitive than their unpatterned precursors, with the extent of reduction being fairly similar for any given vapor; for both arrays larger reductions are observed for TOL and OCT and little or no reduction is observed for POH. In contrast, sensitivities of sensors with the DPA_x films are consistently higher than those with DPA. For sensors with HME_x films, sensitivities increase for the polar vapors and decrease for TOL and OCT relative to those with (unpatterned) HME films.

In general, while the sign and magnitude of sensitivity changes differ among the different sensors, a preferential sensitivity to polar vapors is consistently observed among the patterned films relative to their unpatterned precursors (see Figure 2c,d). Note, in particular, the reversal in the relative sensitivities to TOL and POH between unpatterned and patterned films. Exposure to ambient air after EBIX has been shown to generate oxygenated species in self-assembled monolayers by quenching residual radicals or adding across sites of unsaturation created during exposure.[30] The incorporation of oxygenated species into the ligands (e.g., —OH, —OR, or —COOH) would increase the affinity of polar vapors for the MPN films and could account for the observed sensitivity trends.

In our previous study, $C8_x$ films also showed greater sensitivity toward polar vapors than nonpolar vapors (relative to C8), but
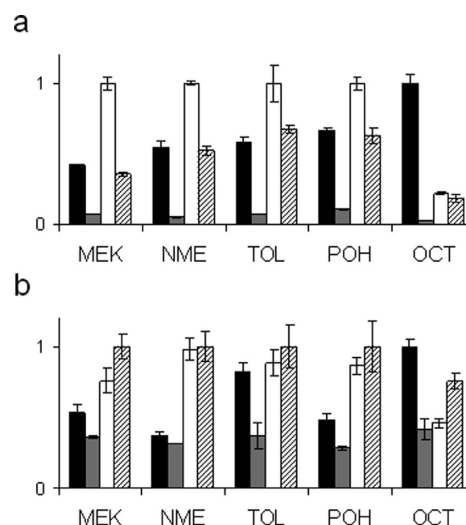
Figure 3. Normalized response patterns for the five test vapors measured with the virtual 4-CR arrays with (a) unpatterned and (b) patterned MPN films: from left to right, C8 ($C8_x$), DPA (DPA_x), OPH (OPH_x), HME (HME_x). Patterns were normalized by dividing each sensitivity value by the highest sensitivity value for a given vapor. Error bars represent one standard deviation above and below the mean sensitivities from the sensors in the mono-MPN arrays.

OPH_x had the opposite trend (relative to OPH). Furthermore, in that study the sensors with patterned films had increased sensitivity to all vapors. The results obtained here for $C8_x$ and OPH_x, thus, differ from those found previously with larger devices. The consistent increases in sensitivity observed here with DPA_x would be explained by an increase in swelling efficiency of the cross-linked ligands, superimposed on the increase in film polarity. Again, by analogy with biphenyl-4-thiol SAMs,[31] reductions in the separation between linked DPA ligands on adjacent MPNs could promote greater interactions with sorbed vapors, leading to improvements in swelling efficiency. With HME_x, the preference for the polar vapors is quite dramatic, strongly suggesting the dissociation of coordinated ester groups on adjacent ligands or hydrolysis of the ester groups, or both.

Vapor Discrimination with Unpatterned and Patterned CR Arrays. Virtual array response patterns for each test vapor were derived from the average vapor sensitivities of the mono-MPN arrays before and after patterning. These are presented as bar charts in Figure 3a,b. For the virtual array with unpatterned films, the response patterns for the polar vapors are qualitatively similar, and quite different from the pattern for OCT, as expected. The response patterns for POH and TOL are surprisingly similar to each other. The OPH sensor is the most sensitive to all vapors except OCT for which C8 is the most sensitive by a considerable margin. The relatively low response from the DPA sensor is evident for all vapors.

For the virtual array with patterned films the response patterns for all vapors change significantly. The qualitative similarity in response patterns among the three polar vapors is still present, despite changes in those patterns. The patterns for TOL and POH are less similar, and for OCT, the $C8_x$ sensor is still the most sensitive, but to a lesser degree than for C8 in the unpatterned array. The DPA_x sensor remains the least sensitive to all vapors, but its relative sensitivity has increased compared to that in the unpatterned array.
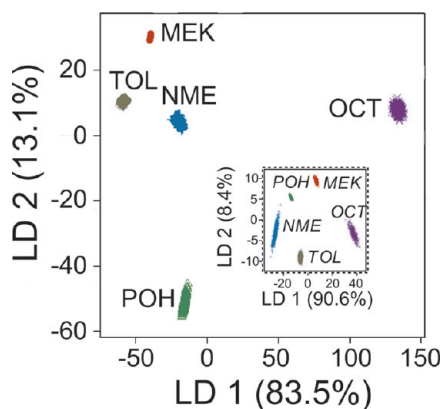
Figure 4. Linear discriminant plots for virtual arrays with unpatterned (main plot) and patterned (inset) MPN films. The inset has been scaled so that the distances spanned among the vector clusters are comparable to those of the plot for the array with unpatterned films. The applied errors used in the Monte Carlo simulations are the RSDs of the sensitivities calculated from three (patterned) or four (unpatterned) different sensors coated with a given type of MPN (4.0%, 3.9%, 5.4%, and 7.2% for C8, DPA, OPH, and HME, respectively, and 8.8%, 8.3%, 14.3%, and 9.7% for $C8_x$, DPA_x, OPH_x, and HME_x respectively). A total of 500 iterations were run for each vapor. (Note that in both LDA plots the distances along the ordinate (y axis) are exaggerated; the amount of variability spanned by the second LDA is, in fact, much smaller than that of the first LDA.)

Two approaches were taken to assess array diversity in more quantitative terms. The first entailed LDA and the second entailed EDPCR. In both cases, Monte Carlo simulations (500 iterations) were used to generate error-enhanced responses that were then classified by LDA or EDPCR. Thus, random (Gaussian) sensitivity error equivalent to the lowest average RSD of the 3 or 4 sensors coated with a given MPN (i.e., based on a single sensor's variability averaged across all vapor calibration points) was applied to the average (normalized) response from each sensor to a randomly selected concentration of each individual vapor within a range defined by 5–10 times the LOD for the vapor. For LDA, each simulated response vector was projected onto the plane created from the first and second linear discriminants. For EDPCR, each vector was projected sequentially onto the plane created from the principal components model for each vapor from calibration, and classification was based on the shortest Euclidean distance.

As shown in Figure 4, both virtual arrays permit discrimination of the individual vapors as reflected by the distinct regions occupied by the vector clusters on the LD projection planes. However, the separation distances are significantly smaller for the virtual patterned array. Indeed, the sum of the Euclidean distances among all the vectors for the virtual array with unpatterned films is 690 while that for the virtual array with patterned films is 270.

EDPCR analyses were used to generate statistical estimates of recognition rates (RRs) for the individual vapors and then for all possible binary mixtures. For tests of individual vapors, the unpatterned array yields an average RR value of 98%, and the patterned array yields a surprisingly high RR of 96%. The recognition matrices (Tables S3 and S4, Supporting Information) show the individual-vapor RR values and shifts in the nature of the recognition errors.

EDPCR analyses of binary mixtures were used to probe the ability of the virtual MPN arrays to distinguish a mixture of two
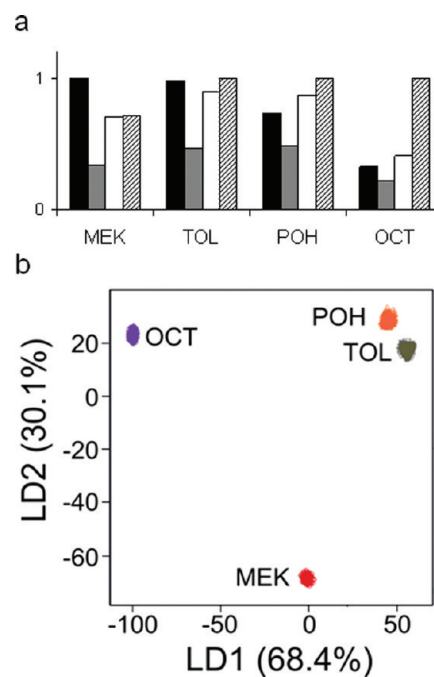

Figure 5. (a) Normalized response patterns from the (patterned) multi-MPN array, with sensitivity values normalized to the highest value for a given vapor: from left to right $C8_x$ (black), DPA_x (gray), OPH_x (white), and HFA_x (crosshatched). (b) LDA plot from multiple-MPN array of data generated by Monte Carlo simulations (500 iterations per vapor) with the following relative errors superimposed on responses from experimental sensitivities: 7.4%, 5.8%, 5.8%, and 4.4% for $C8_x$, DPA_x, OPH_x, and HFA_x, respectively. (Note that data for MEK and POH were reported on previously in ref 5.)

vapors from each of the individual components. All 10 possible binary mixtures were considered in succession. EDPCR models for the binary mixtures were created assuming additivity of responses to each mixture component. The virtual unpatterned array yields an average binary RR of 83%, with specific mixture RRs ranging from 48% to 99% (Table S6, Supporting Information). The virtual patterned array yields comparable results, with an average RR value of 81%, with a range 51–97% (Table S6, Supporting Information). For the unpatterned array, the NME-POH and TOL-POH pairs give particularly low RR values, and bring the overall average down significantly, while for the patterned array, the MEK-POH and NME-POH pairs give the lowest RR values. Fortunately, these pairs of vapors differ sufficiently in vapor pressure to expect facile chromatographic separation, and for cases where only partial chromatographic separation is possible, multivariate curve resolution methods could be used to offset the relatively low binary RRs and increase the likelihood of discrimination of the components.[13]

Patterned Multi-MPN Array Performance. EBIX patterning was then performed sequentially with a different MPN on each of the four sensors in a single multi-MPN array using the same dose as used for the mono-MPN arrays. Notwithstanding the high and variable resistances of unpatterned HFA films, since the acidic proton in the hexafluoro-alcohol moiety of the HFA thiolate has been shown to enhance responses to vapors with Lewis basicity,[34] it was reasoned that it would improve the array diversity if used in place of HME in the multi-MPN array.

The array was calibrated with four individual vapors (NME was omitted): TOL, POH, MEK, and OCT. These sensors also

exhibit rapid, reversible responses to vapor challenges, with full response and recovery achieved in 30 s, with the exception of C8, which requires up to 1.2 min to fully respond or recover, undoubtedly due to this film being thicker than those of the other MPNs. Calibration curves are linear ($r^2 \geq 0.98$), and the sensitivities are 1.2–4.7 times higher than those of the corresponding mono-MPN array values for the three MPNs common to both arrays, with the exception of OCT with C8$_x$, for which the multi-MPN array value is 0.8 times that of the C8$_x$ sensor in the mono-MPN array. Since film thickness should not figure prominently in the sensitivity,[9] it is not clear to us why these sensitivities are generally higher than those of the patterned mono-MPN array sensors.

Like the virtual patterned mono-MPN array, this array exhibits a preferential sensitivity toward POH, and the C8$_x$ and OPH$_x$ films show comparable sensitivities toward MEK and OCT (see Tables S1, Supporting Information). These features support the notion that both C8 and OPH have been rendered more polar by the EBIX process, as found in the virtual mono-MPN array. Furthermore, the DPA$_x$ sensitivities are more similar to those of the C8$_x$ and OPH$_x$ than was the case with the unpatterned films, a feature also found with the virtual patterned mono-MPN array. Normalized response patterns for TOL and POH are similar to those for the virtual patterned mono-MPN array among the 3 sensors common to both arrays, while the patterns for MEK and OCT are quite different (compare Figure 5a to Figure 3b). Thus, both quantitative and qualitative differences between the sensors in the patterned mono-MPN and patterned multi-MPN arrays are evident and can be attributed to differences in the nature and extent of EBIX-induced transformations of the MPN films.

The LDA plot in Figure 5b indicates good separation of the response vectors. The sum of the Euclidean distances among the vectors of the four vapors (350) exceeds that of the virtual patterned mono-MPN array (150, excluding NME), reflecting the benefit of substituting HFA$_x$ for HME$_x$ in the array. EDPCR analysis gives an average RR of 96% for individual vapor discriminations and 83% for binary mixture discriminations (range 58–98%) with the multi-MPN array (see Tables S5 and S6, Supporting Information). Thus, despite apparent differences in EBIX-induced effects on the films, the expected performance is comparable to that of the virtual patterned mono-MPN array.

CONCLUSIONS

This study has shown that MPNs with a range of different thiolate monolayers can be patterned on densely packed, ultraminiature arrays of CR vapor sensors by EBIX. The EBIX process results in changes to the structures of the thiolate ligands in the MPN films that manifest themselves as changes in the baseline resistance and vapor response characteristics of the sensors. Although response and recovery times did not change, and calibration curves remained linear after patterning, vapor sensitivities changed by 1–5-fold as a result of patterning, with both increases and decreases observed among the four or five test vapors. This indicates that multiple factors are at play, which makes prediction of performance difficult. A general increase in sensitivity toward polar vapors, however, supports the notion that films undergo oxidation upon removal from the electron-beam exposure chamber. Changes in sensitivities and baseline noise levels lead to changes in LODs that vary with the specific MPN and the vapor. Although the reproducibility of responses

among replicate sensors with the same MPN films on a given substrate was reasonably good, responses differed from those obtained with a single array of the same MPNs patterned sequentially on the same substrate and from those obtained in a previous study of EBIX on larger CR devices. Clearly, further work is necessary to identify and control all relevant processing variables.

Chemometric analyses revealed that the diversity of the array responses diminishes after patterning but is still sufficient to permit the discrimination of individual vapors and their binary mixtures with relatively low error, comparable to that estimated with the unpatterned array. That is, in spite of apparent differences in EBIX induced changes in MPN ligand structures as a function of device size and processing variations, vapor discrimination remains high. In a μGC detector configuration, retention times can be used in conjunction with response patterns to differentiate vapors. For fully resolved peaks, response patterns increase the reliability of vapor identification. For partially overlapping peaks, recognition of the vapors involved may require multivariate curve resolution methods to overcome confusion in cases where the response patterns are quite similar.

Importantly, we have demonstrated that an array of MPN coated CRs occupying an area of only 600 μm^2 can provide the response diversity and range of sensitivities required for effective μGC detection. To our knowledge, this is the smallest CR sensor array yet reported. The reduction in detector volume achievable using arrays such as those studied here as compared to those we have reported previously is up to 10^4-fold.[14] This should lead to commensurate reductions in detector dead times and associated band broadening, which are currently limiting factors in microsensor-based μGC detectors.[14,35] On-going work is directed at integrating multi-MPN arrays with EBIX-patterned films into complete μGC prototypes such as those we have reported on recently.[35]

ASSOCIATED CONTENT

S **Supporting Information.** Recognition matrices for individual-vapor discriminations as well as the RR values for all binary mixtures using the unpatterned and patterned CR arrays. Tabulations of detection limits, noise values, and sensitivities. This material is available free of charge via the Internet at http://pubs.acs.org.

AUTHOR INFORMATION

Corresponding Author
*E-mail: ezellers@umich.edu.

ACKNOWLEDGMENT

REFERENCES

(1) Grate, J. W.; Nelson, D. A.; Skaggs, R. *Anal. Chem.* **2003**, 75, 1868–1879.

3694

dx.doi.org/10.1021/ac200019a |*Anal. Chem.* 2011, 83, 3687–3695

(2) Chiu, C. S.; Gwo, S. *Anal. Chem.* **2008**, *80*, 3318–3326.

(3) Sih, B. C.; Wolf, M. O.; Jarvis, D.; Young, J. F. *J. Appl. Phys.* **2005**, *98*, 114314/1–4.

(4) (a) Wohltjen, H.; Snow, A. W. *Anal. Chem.* **1998**, *70*, 2856–2859. (b) Cai, Q. Y.; Zellers, E. T. *Anal. Chem.* **2002**, *74*, 3533–3539. (c) Bohrer, F. I.; Covington, E.; Kurdak, C.; Zellers, E. T. *Proceedings of the 15th International Conference on Solid State Sensors, Actuators, and Microsystems, Transducers '09*, Denver, CO, June 21−25, 2009; pp 148−151. (d) Covington, E.; Turner, R. W.; Kurdak, C.; Rowe, M. P.; Xu, C.; Zellers, E. T. *Proceedings of the IEEE Sensors Conference*, Lecce, Italy, October, 2008; pp 240−242.

(5) Covington, E.; Kurdak, C.; Bohrer, F. I.; Chang, H.; Zellers, E. T. *Lab Chip* **2010**, *10*, 3058–3060.

(6) (a) Wang, L.; Shi, X.; Kariuki, N. N.; Schadt, M.; Wang, G. R.; Rendeng, Q.; Choi, J.; Luo, J.; Lu, S.; Zhong, C. J. *J. Am. Chem. Soc.* **2007**, *129*, 2161–2170. (b) Ibanez, F. J.; Gowrishetty, U.; Crain, M. M.; Walsh, K. M.; Zamborini, F. P. *Anal. Chem.* **2006**, *78*, 753–761.

(7) Joseph, Y.; Peic, A.; Chen, X.; Michl, J.; Vossmeyer, T.; Yasuda, A. *J. Phys. Chem. C* **2007**, *111*, 12855–12859.

(8) Steinecker, W. H.; Bohrer, F. B.; Farina, L.; Rowe, M. P.; Kurdak, C.; Zellers, E. T. *IEEE Sens. J.* **2011**, *11* (2), 469–480.

(9) Steinecker, W. H.; Rowe, M. P.; Zellers, E. T. *Anal. Chem.* **2007**, *79*, 4977–4986.

(10) Kurdak, Ç.; Kim, J.; Kuo, A.; Lucido, J. J.; Farina, L. A.; Bai, X.; Rowe, M. P.; Matzger, A. J. *Appl. Phys. Lett.* **2005**, *86*, 073506/1–3.

(11) (a) Terrill, R. H.; Postlethwaite, T. A.; Chen, C.; Poon, C. D.; Terzis, A.; Chen, A.; Hutchison, J. E.; Clark, M. R.; Wignall, G.; Londono, J. D.; Superfine, R.; Falvo, M.; Johnson, C. S., Jr.; Samulski, E. T.; Murray, R. W. *J. Am. Chem. Soc.* **1995**, *117*, 12537–12548. (b) Wuelfing, W. P.; Murray, R. W. *J. Phys. Chem. B* **2002**, *106*, 3139–3145.

(12) (a) Zellers, E. T.; Park, J.; Hsu, T.; Groves, W. A. *Anal. Chem.* **1998**, *70*, 4191–4201. (b) Hsieh, M. D.; Zellers, E. T. *Anal. Chem.* **2004**, *76*, 1885–1895.

(13) Jin, C.; Zellers, E. T. *Sens. Actuators, B* **2009**, *139*, 548–556.

(14) (a) Lu, C. J.; Steinecker, W. H.; Tian, W. C.; Oborny, M. C.; Nichols, J. M.; Agah, M.; Potkay, J. A.; Chan, H. K. L.; Driscoll, J.; Sacks, R. D.; Wise, K. D.; Pang, S. W.; Zellers, E. T. *Lab Chip* **2005**, *5*, 1123–1131. (b) Kim, S. K.; Chang, H.; Zellers, E. T. *Proceedings of the 15th International Conference on Solid State Sensors, Actuators, and Microsystems, Transducers '09*, Denver, CO, June 21−25, 2009; pp 128−131. (c) Serrano, G.; Chang, H.; Zellers, E. T. *Proceedings of the 15th International Conference on Solid State Sensors, Actuators, and Microsystems, Transducers '09*, Denver, CO, June 21−25, 2009; pp 1654−1657. (d) Zhong, Q.; Steinecker, W. H.; Zellers, E. T. *Analyst* **2009**, *134*, 283–293.

(15) Ancona, M. G.; Snow, A. W.; Foos, E. E.; Kruppa, W.; Bass, R. *IEEE Sens. J.* **2006**, *6*, 1403–1414.

(16) Note that since the baseline noise increases with the inverse square-root of the sensor area,[10,15] the signal-to-noise (S/N) ratio will decrease with sensor miniaturization, but the minimum detectable sorbed vapor mass decreases in proportion to the square-root of the sensor area (assuming the film thickness is constant).

(17) Harnack, O.; Raible, I.; Yasuda, A.; Vossmeyer, T. *Appl. Phys. Lett.* **2005**, *86*, 034108/1–3.

(18) Wang, W. M.; Stoltenberg, R. M.; Liu, S.; Bao, Z. *ACS Nano* **2008**, *2*, 2135–2142.

(19) Werts, M. H. V.; Lambert, M.; Bourgoin, J. P.; Brust, M. *Nano Lett.* **2002**, *2*, 43–47.

(20) Rowe, M. P.; Plass, K. E.; Kim, K.; Kurdak, Ç.; Zellers, E. T.; Matzger, A. J. *Chem. Mater.* **2004**, *16*, 3513–3517.

(21) Porter, M. D.; Bright, T. B.; Allara, D. L.; Chidsey, C. E. D. *J. Am. Chem. Soc.* **1987**, 3559–3568.

(22) Reese, S.; Fox, M. A. *J. Phys. Chem. B* **1998**, *102*, 9820–9824.

(23) Fang, L.; Park, J. Y.; Ma, H.; Jen, A. K. Y.; Salmeron, M. *Langmuir* **2007**, *23*, 11522–11525.

(24) Galbiati, E.; Del Zoppo, M.; Tieghi, G.; Zerbi, G. *Polymer* **1993**, *34*, 1806–1810.

(25) (a) Patrash, S. J.; Zellers, E. T. *Anal. Chem.* **1993**, *65*, 2055–2066. (b) Grate, J. W. *Chem. Rev.* **2000**, *100*, 2627–2648.

(26) Grate, J. W.; Abraham, M. H. *Sens. Actuators, B* **1991**, *3*, 85–111.

(27) Brune, B. J.; Payne, G. F.; Chaubal, M. V. *Langmuir* **1997**, *13*, 5766–5769.

(28) Grolier, J.-P. E.; Ballet, D.; Viallard, A. *J. Chem. Thermodyn.* **1974**, *6*, 895–908.

(29) Yang, C. Y.; Li, C. L.; Lu, C. J. *Anal. Chim. Acta* **2006**, *565*, 17–26.

(30) Seshadri, K.; Froyd, K.; Parikh, A. N.; Allara, D. L.; Lercel, M. J.; Craighead, H. G. *J. Phys. Chem.* **1996**, *100*, 15900–15909.

(31) Geyer, W.; Stadler, V.; Eck, W.; Zharnikov, M.; Golzhauser, A.; Grunze, M. *Appl. Phys. Lett.* **1999**, *75*, 2401–2403.

(32) Turchanin, A.; Kafer, D.; El-Desawy, M.; Woll, C.; Witte, G.; Golzhauser, A. *Langmuir* **2009**, *25*, 7342–7352.

(33) Huels, M. A.; Dugal, P. C.; Sanche, L. *J. Chem. Phys.* **2003**, *118*, 11168–11178.

(34) Grate, J. W. *Chem. Rev.* **2008**, *108*, 726–745.

(35) Chang, H.; Kim, S. K.; Sukaew, T.; Bohrer, F. I.; Zellers, E. T. *Proc. Eurosensors XXIV*, Linz, Austria, September 5−8, 2010; *Procedia Engineering* **2010**, Vol. 5, pp 973−976.

(36) *CRC Handbook of Chemistry and Physics*, 91st ed.; Haynes, W. M., Frederikse, H. P. R., Eds.; Taylor and Francis: New York, 2010; Section 6.